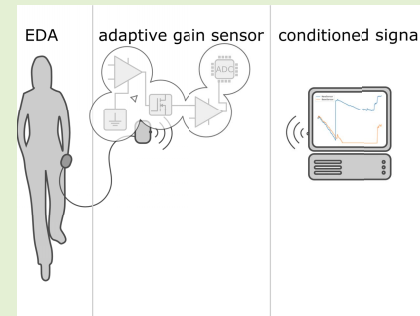


Design and Evaluation of an Electrodermal Activity Sensor (EDA) With Adaptive Gain

António Rodrigues Bangano, Marcelino Bicho dos Santos, *Senior Member, IEEE*,
and Hugo Plácido da Silva, *Senior Member, IEEE*

Abstract—Electrodermal activity (EDA) is a physiological signal that can be measured non-intrusively and associated with the sympathetic nervous system, hence being widely used nowadays. Although multiple sensor designs have been proposed over the years, practical hardware limitations still persist, due to differences in the electrode materials used to interface with the body, sweat gland density at the recording sites, and variability in the overall electrical properties of the skin in-between users. This is particularly challenging when low resolution Analog-to-Digital Converters (ADC) are used, which, due to the proliferation of open source and low-cost hardware platforms, are currently widespread. In this article we present a design and experimental evaluation of a new circuit for EDA measurement with adaptive gain control, allowing the dynamic adaptation of the measurement range. The proposed circuit has shown comparable results to those obtained with a reference sensor, obtaining a mean correlation coefficient of 0.967, and proved to have superior performance in cases where the reference sensor would saturate.

Index Terms—Electrodermal activity (EDA), non-gelled electrode materials, integumentary system, affective computing.



I. INTRODUCTION

THE electrical properties of the human skin vary continuously, as a result of multiple processes mediated directly or indirectly by the Central Nervous System (CNS). Such variations are generally designated as Electrodermal Activity (EDA) and, although partially associated with thermal regulation, they also reflect changes in the behavioral,

Manuscript received December 7, 2020; revised January 7, 2021; accepted January 8, 2021. Date of publication January 11, 2021; date of current version February 17, 2021. This work was funded in part by Fundação para a Ciência e Tecnologia (FCT)/Ministério da Ciência, Tecnologia e Ensino Superior (MCTES) through national funds and when applicable co-funded EU funds under Project UIDB/50008/2020, in part by the IT - Instituto de Telecomunicações under Grant BIL/No. 54 10-07-2018, in part by the Xinhuanet Future Media Convergence Institute (FMCI) under Project S-0003-LX-18, and in part by the Ministry of Economy and Competitiveness of the Spanish Government co-founded by the European Regional Development Fund (ERDF) (PhysComp project) under Grant TIN2017-85409-P. The associate editor coordinating the review of this article and approving it for publication was Dr. Shanhong Xia. (*Corresponding author: Hugo Plácido da Silva*.)

António Rodrigues Bangano is with the Instituto Superior Técnico, 1049-001 Lisbon, Portugal (e-mail: banganoantonio@gmail.com).

Marcelino Bicho dos Santos is with the Instituto Superior Técnico, 1049-001 Lisbon, Portugal, and also with the Instituto de Engenharia de Sistemas e Computadores, Investigação e Desenvolvimento (INESC-ID), 1049-001 Lisbon, Portugal (e-mail: marcelino.santos@tecnico.ulisboa.pt).

Hugo Plácido da Silva is with the Instituto Superior Técnico, 1049-001 Lisbon, Portugal, and also with the Instituto de Telecomunicações (IT), 1049-001 Lisbon, Portugal (e-mail: hsilva@lx.it.pt).

Digital Object Identifier 10.1109/JSEN.2021.3050875

cognitive and emotional state of an individual [1]–[4]. For this reason, the EDA is known as an indirect observation of the Sympathetic Nervous System (SNS), being used as biomarker in behavioral medicine, affective computing, neurosciences and related areas [5]–[8].

Generally, EDA signals related with the SNS activity are more noticeable at the hand palms and foot soles and have two components, the tonic and the phasic [1], [9], [10]. The tonic component is considered to be the slowly varying baseline of the signal, while the phasic component is considered to be the rapidly changing events that superimpose the baseline, frequently fluctuating according to a known elicitation of a particular stimulus.

With the rise in popularity of low cost and open source hardware platforms for biomedical applications [11], EDA sensing is increasingly used by students, researchers, and professional developers in numerous prototyping activities for which off-the-shelf devices (e.g. wearables) are too restrictive [12], [13]. However, multiple challenges still exist in this approach.

The tonic component typically ranges between 0 and $80\mu\text{S}$, while the phasic component has a much lower scale (0.01– $5\mu\text{S}$); combined with the low resolution of Analog-to-Digital Converters (ADCs) used in the most common open source hardware platforms (e.g. the Arduino), this leads to a limited ability to measure the phasic component. Furthermore, the sensors are typically applied on the hand palms or feet soles in conjunction with pre-gelled electrodes; changes in

the sensor location and/or electrode materials greatly affect the measurement ability of the standard fixed gain sensors.

In this work we propose a design and experimental characterization for a sensor that provides greater flexibility in EDA signals measurement, especially when using low resolution ADCs, by allowing a digitally controlled gain adaptation. The remainder of this work is organized as follows. Section II provides an overview of related work and further reinforces the existing challenges. Section III describes the main aspects of the proposed sensor design. Section IV presents the experimental results for a comparative evaluation against a reference sensor. Finally, Section V outlines the main conclusions and envisioned future work directions.

II. BACKGROUND

A. State of the Art

Multiple sensors, platforms and devices for EDA measurement have already been created and made commercially available.

MySignals, developed by Libelium's Cooking Hacks,¹ is a medical development platform oriented for researchers, and compatible with standard open source hardware. On a more off-the-shelf approach, the Empatica E4 wristband [14], [15] is a wearable research device that offers real-time physiological data acquisition hardware and software for in-depth analysis and visualisation.

GSR 2, developed by Thought Technology,² is a small, hand-held and self-contained EDA monitoring device for home biofeedback. Also, from Thought Technology, the eVu-TPS sensor,³ is a portable sensor that enables heart rate and EDA data acquisition outside the clinical environment using mobile devices.

From BIOPAC Systems, the EDA100C Electrodermal Activity Amplifier,⁴ is an EDA amplifier focused on research applications. Their BioNomadix Transmitter,⁵ also combines a wireless Photoplethysmography (PPG) and EDA sensor to enable simultaneous recording of blood volume pulse and electrodermal activity.

The Shimmer3 GSR,⁶ is a realtime EDA biofeedback device, which offers the possibility of adding other sensors (e.g. Shimmer photoplethysmogram). Lastly, The MindMedia Skin Conductance Sensor⁷ is another commercially available option.

Most of the devices mentioned above, record the EDA signal in zones that represent an obstruction to movement or comfort of the wearer, which is a limiting aspect when conducting long-term measurements. Furthermore, the use of pre-gelled electrodes is generally mandatory or recommended.

¹http://www.libelium.com/downloads/documentation/mysignals_technical_guide.pdf

²<https://thoughttechnology.com/index.php/hardware/gsr-2.html>

³<https://thoughttechnology.com/index.php/hardware/tps-evu-package-t4500.html>

⁴<https://www.biopac.com/product/eda-electrodermal-activity-amplifier/>

⁵<https://www.biopac.com/product/bionomadix-wireless-ppg-and-eda-transmitter/>

⁶http://www.shimmersensing.com/images/uploads/docs/GSR%2B_User_Guide_rev1.13.pdf

⁷<https://www.mindmedia.com/en/products/sensors/skin-conductance-sensor/>

Authors like Poh in [16] or Pope *et al.* in [17] attempted to address this problem, designing a wristband that performs EDA measurements on the wrist area.

Other research worth mentioning includes the work from Picard & Scheirer [18], whom developed a glove called Galvactivator that maps the skin conductivity onto a LED. Lee *et al.* [19] proposed a sensing glove using conducting fabric and an embedded system. The iCalm sensor [20] is characterized for being a low-power and a wireless platform that can be integrated into a wristband or sock. Lastly, we also highlight the work presented by Sousa *et al.* [21], in which a glove capable of measuring PPG and EDA data is presented.

On a more consumer-oriented segment, existing work includes The Pip⁸ or even the Moodmetric ring [22], which combines biosignal sensors, such as EDA, with machine learning algorithms to extrapolate an index value of the user stress levels.

Over the past years there has been a rapid increase in low-cost and open hardware alternatives [11]. Within this segment, BITalino [23] has been recently released as a scientifically validated low-cost open source hardware and software toolkit for biosignal acquisition, hence being the platform used as the base for the present work [24], [25].

B. Main Limitations

The high costs associated with professional research equipment, and limited access to raw data and specialization in a particular application in the case of off-the-shelf devices, have hindered the widespread use of EDA sensors. Existing low-cost alternatives lack the ADC resolution and sensitivity. Furthermore, the recommended sites for sensing EDA are limited to the hand palm area and the foot area, since they present a higher density of sweat glands per cm² [26].

However, these locations significantly reduce the freedom of movement of the subjects, constituting a constraint for the application to wearable devices that might otherwise integrate EDA sensors. Moving the electrodes to less intrusive locations greatly influences the measurement range of the signal. Table I presents a summary of the commercial systems most commonly found in the state of the art and their main characteristics.

As shown, the measurement range is quite broad. Considering, for example, a worst-case scenario of a MindMedia sensor used with a 10-bit ADC, the step size would be approximately 1 μS. Taking into account the typical ranges for the tonic and phasic components described in Section I, most of the useful information in the EDA signal would be masked. This limitation was further reinforced by empirical evidence gathered in the scope of our work.

We analyzed a real world dataset collected by neuroscience company BrainAnswer⁹ using BITalino equipment [24], containing, amongst other modalities, EDA data acquired from 99 participants during a cognitive elicitation experiment. The objective of this analysis was to further assess the need for an EDA sensor with adaptive gain. From the 99 recordings,

⁸<https://thepip.com/en-eu>

⁹<https://brainanswer.pt/>

TABLE I
MOST COMMON COMMERCIAL SYSTEMS FOR EDA MEASUREMENT AND THEIR SPECIFICATIONS

Device	Electrode Position	Electrode Type	Measurement Range	Bandwidth
BITalino	Unrestricted	Ag/AgCl	0-25 μ S	0-2.8Hz
MySignals	Medial & distal phalanx	Ag/AgCl with velcro	0-20 μ S	
Empatica E4	Bottom wrist	Ag/AgCl with ABS core	0.01100 μ S	
GSR 2	Medial & distal phalanx	Ag/AgCl	1k-3M Ω	
eVu-TPS	Medial & distal phalanx	Stainless Steel	0-30 μ S	
EDA100C	Unrestricted	Ag/AgCl	0-200 μ S	
BioNomadix	Unrestricted	Ag/AgCl with velcro	0-50 μ S	0-3Hz
Shimmer3	Medial & distal phalanx	Snap connector Ag/AgCl electrodes	0.2-125 μ S	0-15.9Hz
MindMedia EDA	Medial & distal phalanx	Ag/AgCl with velcro	0.1-1000 μ S	

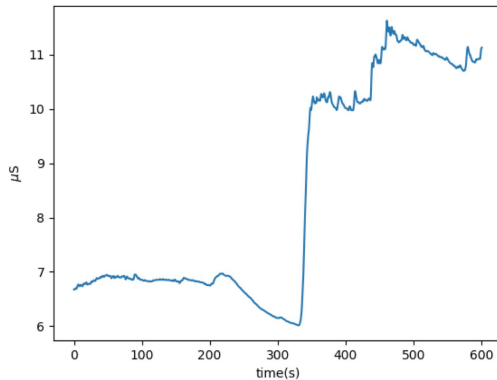


Fig. 1. Example of a normal EDA signal trace.

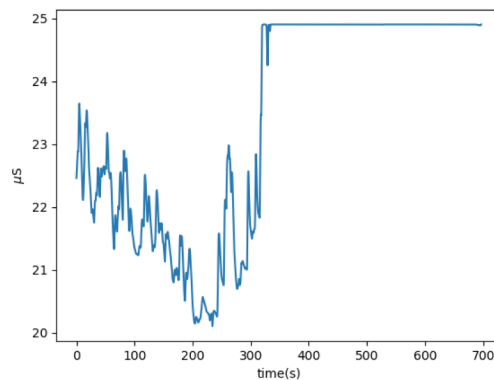


Fig. 2. Example EDA signal trace with a saturated segment.

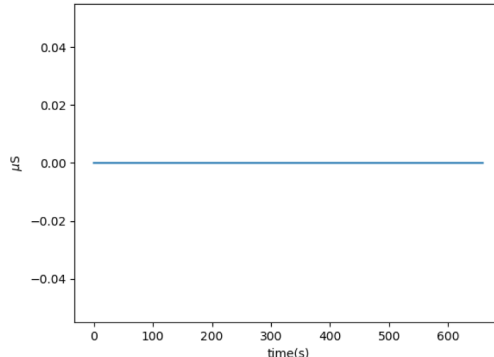


Fig. 3. Example EDA signal showing lack of response.

we quantify the signal, extracting temporal metrics (e.g. mean value, max value, range, and others) to empirically characterize the operation of the sensor. Namely, we evaluate how many subjects exhibit full scale saturation, lack of response (e.g. due to high skin impedance), among other factors.

The sensor leads were applied at the distal phalanx of the index and middle fingers, and the electrodes were the pre-gelled polymer Ag/AgCl coated H124G model from Covidien.¹⁰ Although not particularly relevant for this analysis, elicitation was performed using a set of cognitive demanding tasks. After an initial baseline recording, participants were asked to complete a Stroop word-colour matching test and a geometric combination game.

An example of a normal EDA signal randomly selected from the BrainAnswer database is presented in Figure 1, and examples of EDA signals with full-scale saturation and lack of response (extracted from the same database) are presented respectively in Figures 2 & 3. Table II presents a summary of signal evaluation statistics across the database. From all the recordings, six signals present full-scale saturation while one presents a lack of response. From those six saturated signals, four present saturation in over 80% of the recording session, while the signal that presented lack of response does not present variations throughout the session. The mean and median of all 99 signals is approximately 10.56 μ S, and the range is approximately 4.5 μ S. As for the variance and standard deviation of the signals, it is approximately 1.5 and 1 μ S. All

this information leads us to conclude that an electrodermal activity sensor with an adaptive gain is beneficial.

III. PROPOSED APPROACH

A. Overview

The workflow of an EDA measurement system has different variations, depending on the method used. In the most basic form, EDA measurement requires electrodes to be placed on a location at the skin of the subject, filtering (in order to mitigate artifacts or other unwanted signals), amplification, an ADC, and, finally, a device to record and/or display data. If the gain of the sensor is fixed, the ADC resolution emerges as a bottleneck (as shown in Section II).

Although one can argue that, to solve such limitation, it would simply be necessary to increase the number of bits on the ADC, this has an impact on the complexity and cost of the

¹⁰<https://cdn.sparkfun.com/datasheets/Sensors/Biometric/H124SG.pdf>

TABLE II
STANDARD SENSOR CHARACTERIZATION, EXPRESSED IN μS UNLESS OTHERWISE NOTED

Mean	Median	Variance	Std. Dev.	Range	Max.	Min.	#Fullscale	#Zero
10.563	10.555	1.408	1.002	4.534	13.092	8.558	6.000	1.000

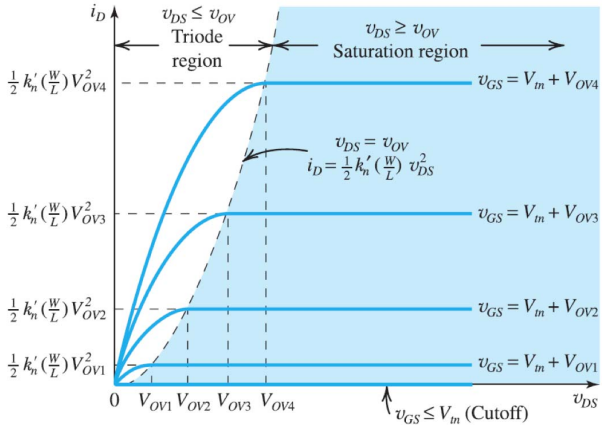


Fig. 4. N-MOSFET operating regions [27].

final system. In our approach we use a N-MOSFET, namely the Nexperia PMV16XN, operating in the triode region, which means that it behaves like a voltage-controlled resistor. This provides the ability to adapt the amplification stage of a sensor, even dynamically.

Figure 4 presents the regions of operation that one can identify in a N-MOSFET. When the applied voltage between gate and source (V_{GS}) is not enough to overcome the threshold voltage (V_{th}), the N-MOSFET is said to be in the cutoff region, where little to no current flows from the drain to the source. To be in the saturation region, two conditions must be met. First, the voltage from gate to source must be higher than the V_{th} , to induce a channel between the gate and source. Secondly, the voltage drain to source (V_{DS}) must be higher or equal than $V_{GS} - V_{th}$. In this region, in a first order approach and ignoring the channel length modulation, I_D can be estimated using Equation 1 (k_n , W , and L are fabrication parameters of the N-MOSFET as established by the manufacturer), where V_{OV} is the overdrive voltage, which can be defined as $V_{GS} - V_{th}$.

$$I_D = \frac{1}{2} k_n \frac{W}{L} V_{OV}^2 \quad (1)$$

With an increase of V_{OV} , I_D will be higher, and vice-versa, and that is why, in this region, the N-MOSFET is considered to behave as a voltage-controlled current source. Lastly, the triode region (sometimes referred to as linear region), is the region in which our N-MOSFET operates. To be in this region, V_{GS} must also overcome V_{th} , but now, V_{DS} must be lower than V_{OV} . In the triode region, the N-MOSFET drain current can be approximated by Equation 2. For a constant V_{OV} , this equation shows two contributions for the drain current: one proportional to V_{DS} , and the other quadratic with V_{DS} . However, taking into account that V_{DS} is limited in this operating region ($V_{DS} < V_{OV}$), the dominant contribution for I_D is the linear one. This

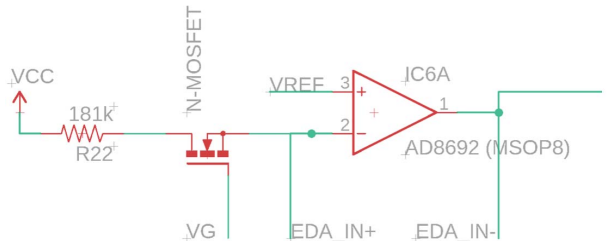


Fig. 5. Proposed circuit for EDA measurement.

is the reason for calling this operating region “linear”. It is also the reason why it is the preferred one for a MOS transistor that is used as a controlled resistance. Figure 4 shows the near linear increase of I_D for low V_{DS} values. In this part of the linear region, since the dominant, V_{DS} proportional, contribution to the drain current can be controlled by V_{OV} , the MOS device behaves as voltage-controlled resistance.

$$I_D = k_n \frac{W}{L} (V_{OV} - \frac{1}{2} V_{DS}) V_{DS} \quad (2)$$

B. Adaptive Gain Control

The proposed circuit for adaptive EDA measurement is presented in Figure 5. It is based on a classic solution [28], to which we added an N-MOSFET transistor with the purpose of gaining control of the current value that is forced during the measurement. Without the N-MOSFET, the EDA measurement can only be performed if the current $(V_{CC} - V_{REF})/R_{22}$ can be forced without saturation of the amplifier. The purpose of adding the N-MOSFET to the circuit is to extend the dynamic range of the sensor, by having control of the current being forced instead of using a fixed one.

While the amplifier is in the linear region, the current in the transistor is very well defined, since its source is at a known voltage (V_{REF}) and, in our approach, the gate is controlled by a Digital-to-Analog Converter (DAC). The DAC defines the appropriate current (see Figure 6), allowing a linear operation of the circuit. In our implementation a DAC controlled by an 8-bit Pulse Width Modulation (PWM) output signal from BITalino is used, therefore V_G is controlled in steps of $12.9mV$ (3).

It is important to notice that linear operation is required in the amplifier, in order to correctly translate the conductivity variations into voltage variations, but the N-MOSFET region of operation is not relevant for the circuit functionality. The N-MOSFET action is to control the current in its branch and it is able to do it either as a voltage-controlled current source (in saturation) or as a voltage-controlled resistance (in the triode).

Once V_G is defined, the current in the N-MOSFET is also defined by: $I_D R_{22} + V_{DS} = V_{CC} - V_{REF}$ and $I_D(V_{DS}, V_G)$, where $I_D(V_{DS}, V_G)$ can be the dependence in saturation or

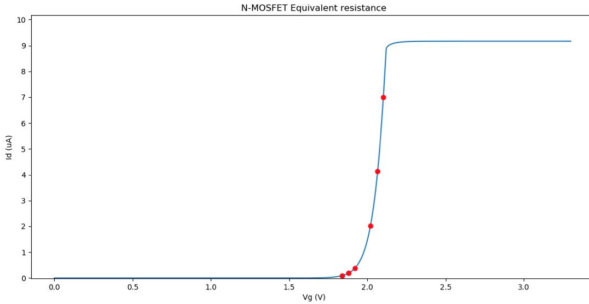


Fig. 6. Relation between V_G and I_D .

in triode. Independently of the linearity of the N-MOSFET operation, the amplifier will adjust the output voltage to produce the current between EDA_IN- and EDA_IN+ identical to the current defined by V_G in the N-MOSFET branch.

$$\Delta V = \frac{3.3}{2^{n_{bits}=8} - 1} = 12.9mV \quad (3)$$

Figure 6 presents the relationship between the applied gate voltage V_G and the current I_D flowing at the drain. The red dots represent the points where the N-MOSFET has an equivalent resistance of $20\text{M}\Omega$, $10\text{M}\Omega$, $5\text{M}\Omega$, $1\text{M}\Omega$, $500\text{k}\Omega$, $300\text{k}\Omega$, modeled according to Equation 4. As shown, the current flowing through the skin does not exceed the maximum recommended current of $10\mu\text{A}/\text{cm}^2$ for DC techniques [26], ensuring that the sweat glands are not damaged. This is achieved thanks to the $R_{22} = 181\text{k}\Omega$ resistor that is in series with the N-MOSFET.

$$R_{MOSFET} = \frac{V_{REF}}{I_D} \quad (4)$$

The current that flows in the EDA sensor (I_{EDA}) can be controlled by R_{MOSFET} according to Equation (5).

$$I_{EDA} = I_{MOSFET} = \frac{V_{CC} - V_{REF}}{R_{MOSFET} + R_{22}} \quad (5)$$

The voltage that results at the output of the sensor depends on the skin measured resistance (R_{EDA}) and on the forced current, as described by Equation (6).

$$V_{EDA} = V_{REF} - I_{EDA}R_{EDA} \quad (6)$$

Based on Equations (5) and (6), the sensor output voltage dependence on the sensed resistance can be obtained (7).

$$V_{EDA} = V_{REF} - R_{EDA} \frac{V_{CC} - V_{REF}}{R_{MOSFET} + R_{22}} \quad (7)$$

Figure 7 shows the sensor output voltage dependence on the sensed resistance for three different R_{MOSFET} values. This figure also shows the dynamic range for measuring R_{EDA} , assuming that the output of the sensor can be quantified in the range $[0V; 1V]$. This example illustrates the importance of selecting the right slope for $V_{EDA}(R_{EDA})$ in order to maximize the dynamic range. The fact that the selection of the dynamic range also impacts $\frac{d(V_{EDA})}{d(R_{EDA})}$ affects the sensitivity of the phasic EDA component, reducing it when larger R_{MOSFET} values are required. The next section presents a solution for the amplification of the phasic component.

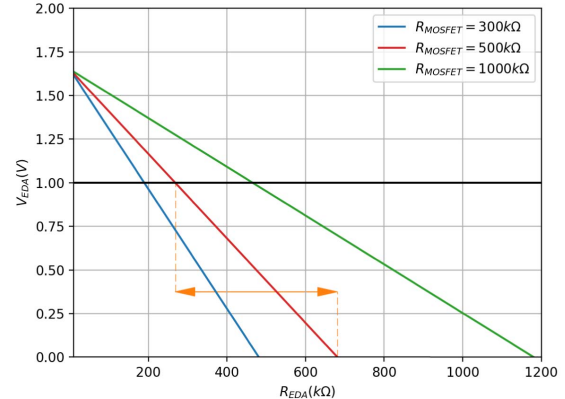


Fig. 7. V_{EDA} as function of R_{EDA} for $V_{CC} = 3.3V$ and $V_{REF} = 1.65V$. Dynamic R_{EDA} range marked for V_{EDA} range of $1V$ and $R_{MOSFET} = 500\text{k}\Omega$.

With this implementation, the circuit now has an adaptive dynamic range; depending on the situation, it can reduce its dynamic range from the original $1\text{M}\Omega$ downwards, or it can increase it above the $1\text{M}\Omega$ limit.

C. Phasic Component Isolation

To address the sensitivity decrease with an increase of the N-MOSFET equivalent resistance value, the proposed sensor design applies a similar method to that found in [29]. Namely, a 2nd order Sallen-Key high-pass filter is implemented, with a cutoff frequency of 10mHz and a stop-band frequency of 1mHz , selected based on the typical EDA frequency response. This enables the separation of the phasic component from the remaining signal. Figure 8 presents the final proposed circuit design, with a gain of 34 dB in the phasic component filtering stage. Since the EDR events have much lower amplitude than EDL, separating the components allows to individually apply different gains. Although the high pass filter section does not have adaptive gain, contrary to the low pass configuration, it can be easily modified since it only depends on resistors.

As described in Section III-B, the sensor uses the BITalino MCU PWM and DAC peripherals to adjust the N-MOSFET (R_{23}) according to software-controlled inputs. Three MCU input channels are used to acquire data from the sensor, one at the output of the low-pass filter (A3), which acquires the EDA signal trace aggregating the tonic and phasic components, another at the output of the high-pass filter, which extracts the phasic component, and, finally, the applied gate voltage (V_G) is monitored on the third input, to enable the computation of the transfer function in post-processing.

With this setup, a control logic can be implemented on the receiver by reading the channel connected to the A3 node and, if the mean of the signal is below a defined threshold (e.g. 5% full scale), the PWM level will be decreased. On the other hand, if the mean value is higher than a defined threshold (e.g. 95% full scale), the PWM level will be increased. The sensitivity varies with the gain of the sensor; in particular, when the equivalent N-MOSFET resistance is very high, it means that the sensitivity offered by the 10-bit ADC will

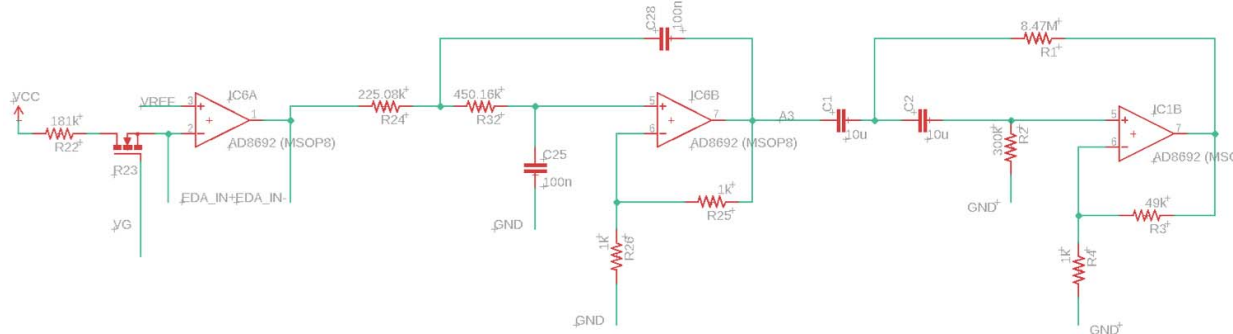


Fig. 8. Final circuit of the proposed sensor.

still not be enough.

$$\Delta R = \frac{RMOSFET}{2^{n_{bits}=8} - 1} \Omega \quad (8)$$

According to Equation 8, if $RMOSFET$ has an equivalent resistance value of $5M\Omega$, each value of the DAC will represent a step of $4.9k\Omega$, which means that small EDR events cannot be detected; this effect continues to worsen as we increase the N-MOSFET equivalent resistance. This is one of the reasons for introducing the high-pass filter, which will isolate those frequencies that carry EDR information.

Finally, the N-MOSFET gate voltage at any given stage is recorded, so that the user can calculate the N-MOSFET equivalent resistance value (Equation 4) throughout the measurement session. This will allow the application of the correct transfer function in post-processing, to convert the raw ADC units to conductance units.

D. N-MOSFET Behaviour

The use of the N-MOSFET in the triode region to simulate the behavior of a potentiometer can be challenging at times, especially when using a PWM signal that is filtered through the use of a DAC.

When changing the gate voltage of the N-MOSFET, there is lag between the input and the output (e.g. VD to VS). This is important to consider when applying the transfer function, because what is seen by the MCU input connected to the gate of the N-MOSFET will not correspond to the actual output of the N-MOSFET during a particular time frame. Simulating the real conditions that this sensor will encounter, we fed the N-MOSFET gate with a PWM level, made it oscillate following a square wave pattern, and monitored the input and output of the N-MOSFET.

Figure 9 shows a mean delay of 9.393ms delay between input and output. According to Figure 10, the rise and fall time of the input was of 44ms and 47ms, respectively. Additionally, it was possible to see that the N-MOSFET or the DAC have some variation at a particular level when a resistance of $1M\Omega$ and $100k\Omega$ are used to simulate a skin resistance.

We could calculate the individual equivalent resistance value of N-MOSFET at a particular level of PWM, but since the transition from one level to the other is not ideal, it is difficult to predict the equivalent resistance during the transition period

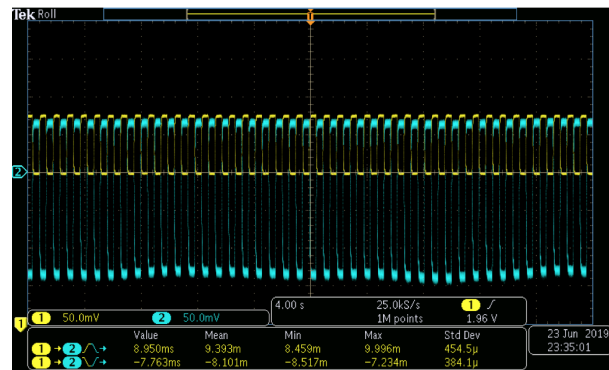


Fig. 9. N-MOSFET response time.

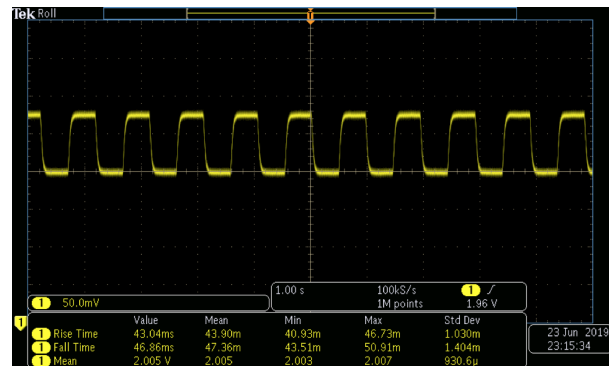


Fig. 10. Characterization of the N-MOSFET output rise and fall times.

from level to level. This further reinforces the importance of continuously monitoring the input gate voltage and taking into account the offset introduced by the delay between the input and output of the N-MOSFET.

E. Calibration Procedure and Dynamic Transfer Function

In order to calculate the correct equivalent N-MOSFET resistance, the circuit has implemented an additional segment on the first stage comprised of two resistances of $1M\Omega$ and $100k\Omega$ with 1% tolerance and a dual 4-channel analog multiplexer/demultiplexer HEF4052B from NXP.

The circuit uses the two digital outputs present in the BITalino acquisition board to select the input to output of the demultiplexer, which, according to Figure 5, has as inputs the

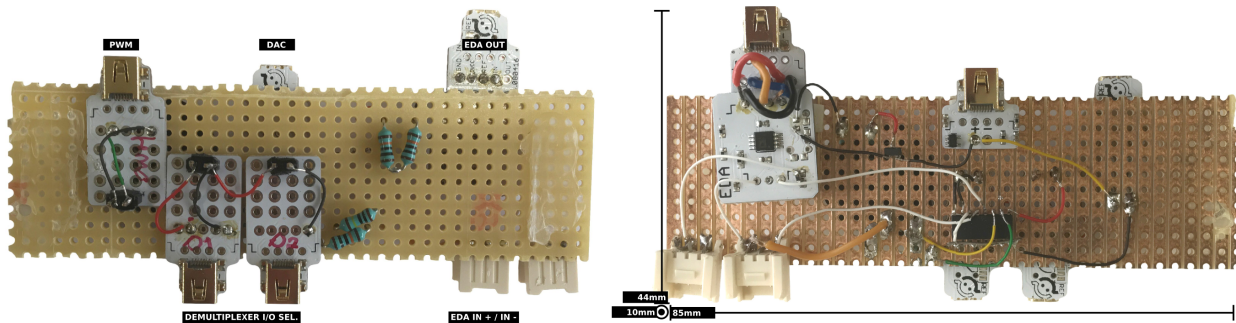


Fig. 11. Hardware prototype of the circuit for use with BITalino.

EDA IN-, a $100\text{k}\Omega$ resistor in parallel between EDA IN- and EDA IN+, and another resistor of $1\text{M}\Omega$ in parallel with the other $100\text{k}\Omega$ resistor.

The HEF4052B then connects only one resistor at the time to the second stage of the circuit, which, according to the selected combination of the HEF4052B, will allow a current flow across the electrodes either through the $100\text{k}\Omega$ or through the $1\text{M}\Omega$ resistor. The calibration procedure involves calculating the equivalent resistance, R_{23} ; knowing the resistance value, we have:

$$R_{23} = \frac{R_{skin} - V_{REF}}{\frac{V_{out} \times V_{CC}}{(2^{nbits}-1) \times G} - V_{REF}} \quad (9)$$

Simulating R_{skin} with resistances enables the calculation of R_{23} at a particular PWM level. The proposed circuit implements a very simple logic at the beginning of an acquisition; it first measures the skin resistance level of the user and then changes the current flow from the electrodes to the suitable resistance.

If the target skin has a skin resistance higher than $1\text{M}\Omega$, the selection controls change the current flow so that the $1\text{M}\Omega$ resistor is used; it then cycles through PWM levels around the target skin resistance and records the R_{23} , so the system later knows the corresponding R_{23} for a particular PWM level. The same procedure is used when the skin resistance is lower than $1\text{M}\Omega$.

This process can be long since, as shown in Section III-D, the N-MOSFET does not shift immediately and therefore the system has to wait for stabilization between changes of PWM levels applied to the gate N-MOSFET. To save time, we reduced the calibration procedure to take only 3 to 4 seconds, and measuring the R_{23} at reference points close to the user skin resistance, extrapolating the values in-between. After the calibration procedure, the measurement of the subject EDA can start.

IV. EXPERIMENTAL RESULTS

A. Participants

Data was collected from 16 volunteers (5 female and 11 male), with ages comprised between 23 and 39 years, while completing a 4-minute protocol consisting of a baseline, a reflex elicitation task, and a recovery period. The objective was to stimulate the SNS in a reflex manner; according to [30], there are several possibilities to achieve that, namely

through the elicitation of cardiovascular reflexes induced by tasks such isometric exercises, mental arithmetic, cold pressor test, Valsalva manoeuvre, and/or others.

In our experiment, the chosen task was the isometric hand-grip test, due to the simplicity of deployment. Participants had to sustain their grip strength above one-third of the maximum voluntary contraction (determined in an initial step of the protocol), during 3 to 5 minutes. This causes an increase in the diastolic blood pressure that originates from the heart rate acceleration. An interesting fact is the possibility of the patient performing the Valsalva manoeuvre simultaneously, during the task, which can further stimulate the SNS. Nevertheless, since we are focused on comparing the two sensors under evaluation, the possibility of existing a Valsalva manoeuvre is not critical, since its effects will be recorded in both devices.

Informed consent was obtained from all participants before the beginning of the experiment. None of the participants declared to have any physiologically related condition, nor being on medication that could alter their autonomic nervous system at the time of the recording.

B. Materials

The EDA was recorded as skin conductance changes with both sensors used in the experiment (the proposed and reference sensor), at the middle and proximal phalanges of the index and ring fingers, on the non-dominant hand. The practical implementation of the circuit is shown in Figure 11. The reference sensor was attached to the index finger while the proposed sensor to the ring finger. Dry Ag/AgCl electrodes from Thought Technologies with embedded velcro straps were used to ensure that the 1cm^2 area of the electrodes was in contact with the skin at all time. No skin pretreatment nor conductive paste was used. Each sensor was separately attached to an independent BITalino board and data was acquired with a 1000Hz sampling frequency.

In order to guarantee electrical isolation between both sensors, two separate acquisition units were used (one for each sensor), and synchronization was performed optically employing a LED turned on/off on one of the units and a light sensor (LUX) on the other. In post-processing, the time series were aligned by detecting the onset on the LED trigger channel and on the LUX sensor output, removing afterwards the period until those points were found in each of the recorded files. Given that the LUX sensor only changes its

TABLE III

EXTRACTED SIGNAL PROPERTIES, EXPRESSED IN ADC UNIT (0-1023). FOR EACH SUBJECT, THE BOTTOM LINE CORRESPONDS TO THE REFERENCE SENSOR AND THE TOP LINE TO THE PROPOSED CIRCUIT

Subject	Mean	Median	Max	Variance	Std. Deviation	Onsets	P-Coeff	RMSE
Subject 1	522.881	524.000	141.881	2849.777	53.383	44.000	0.981	0.193
	694.034	693.000	95.034	1222.731	34.968	47.000		
Subject 2	700.649	703.000	99.649	1597.493	39.969	53.000	0.956	0.298
	726.555	728.000	93.555	1210.280	34.789	55.000		
Subject 3	479.530	490.000	95.470	2965.529	54.457	52.000	0.986	0.165
	737.529	739.000	39.471	343.029	18.521	52.000		
Subject 4	556.742	594.000	515.742	38671.901	196.652	1.000	-0.475	1.718
	111.042	0.000	355.958	22860.485	151.197	5.000		
Subject 5	733.669	756.000	130.669	3030.999	55.055	52.000	0.891	0.468
	973.043	980.000	38.043	146.333	12.097	8.000		
Subject 6	843.369	844.000	58.631	477.825	21.859	27.000	0.985	0.174
	586.524	591.000	122.476	2190.088	46.798	26.000		
Subject 7	756.034	769.000	109.034	1976.509	44.458	46.000	0.967	0.257
	976.873	978.000	24.873	88.442	9.404	61.000		
Subject 8	324.660	327.000	137.660	6664.945	81.639	38.000	0.985	0.171
	752.630	759.000	62.630	1097.607	33.130	42.000		
Subject 9	395.185	404.000	106.815	3219.526	56.741	36.000	0.996	0.089
	572.059	577.000	87.941	2197.239	46.875	34.000		
Subject 10	795.788	801.000	76.788	905.291	30.088	32.000	0.973	0.232
	780.638	784.000	59.638	592.679	24.345	33.000		
Subject 11	238.309	233.000	213.691	2160.283	46.479	25.000	0.967	0.258
	461.630	458.000	139.370	871.567	29.522	22.000		
Subject 12	683.726	680.000	23.274	141.270	11.886	43.000		
	0.000	0.000	0.000	0.000	0.000	0.000		
Subject 13	556.449	571.000	139.449	2462.090	49.619	24.000	0.989	0.146
	518.140	536.000	168.140	4110.590	64.114	20.000		
Subject 14	570.587	579.000	169.587	3136.935	56.008	41.000	0.972	0.236
	727.865	742.000	115.865	1397.818	37.387	39.000		
Subject 15	470.395	475.000	53.395	242.992	15.588	25.000	0.941	0.344
	709.718	711.000	30.718	94.414	9.717	28.000		
Subject 16	572.156	567.000	83.844	601.608	24.528	20.000	0.955	0.302
	653.329	650.000	69.671	363.811	19.074	14.000		

output when the LED is turned on, and that both signals are synchronously acquired with the EDA data channels, this procedure guarantees that the data is synchronized.

C. Proposed Circuit Evaluation

To compare the signals collected with the reference and experimental sensors, we extracted eight signal properties, summarized in Table III, where the proposed sensor values are presented in the first row out of the two of each subject. In this first assessment, we focused on two particular properties, namely, the Pearson correlation coefficient and the RMSE, which implies that the signals are normalized. Excluding the two cases where some sort of artifact induced by saturation is present, the mean Pearson coefficient was 0.967 with a mean RMSE of 0.238, which can be interpreted as a strongly correlated signal with good point-to-point amplitude matching.

Subjects 4 and 12 both present saturation artifacts in the measurements performed with the standard sensor, illustrating how the new sensor is capable of measuring a wider range of EDA signals. In Subject 4, the EDA is slowly decreasingly with time until the reference sensor is no longer capable of measuring it, which in turn means losing information between time instants 90 and 225 seconds. On the other hand, the control logic for the new sensor detects that the EDA signal is decreasing and close to reaching saturation, increasing the equivalent resistance of the N-MOSFET. This dynamically changes the gain of the sensor, hence the abrupt change on

the EDA signal obtained with the new sensor between 65 and 75 seconds into the recording. Since we record the equivalent N-MOSFET resistor value continuously, we can determine the actual transfer function that should be applied, and this way, the artifact induced by changing the level of the N-MOSFET can be eliminated.

In subject 12, the reference sensor could not read the actual EDA of the participant. The reason for this is that this participant has a skin resistance higher than $1\text{M}\Omega$. Once again, the control logic of the new sensor took advantage of its adaptable characteristics, changing the N-MOSFET equivalent resistance to a more adequate value, which enabled the recording of the EDA. However, at a certain level, especially above the $3\text{M}\Omega$ N-MOSFET equivalent resistance value, the 10-bit ADC does not enable the distinction of the EDR component in the EDA signal. In this case, the implemented third stage, namely the high-pass filter with a 34 dB gain, separates the two components and solely amplifies the EDR component. Analyzing the EDR obtained from Subject 12, we see that although with small amplitude, there are a few peaks that correspond to an EDR. Ultimately, the obtained EDR can be superimposed to the EDA obtained in the above mention conditions to recreate the signal that one would obtain using an ADC with higher resolution.

The overall obtained signals of the 3rd stage exhibit cases of data corruption induced by saturation, cases where no saturation occurs, and cases where almost no fluctuation exists.

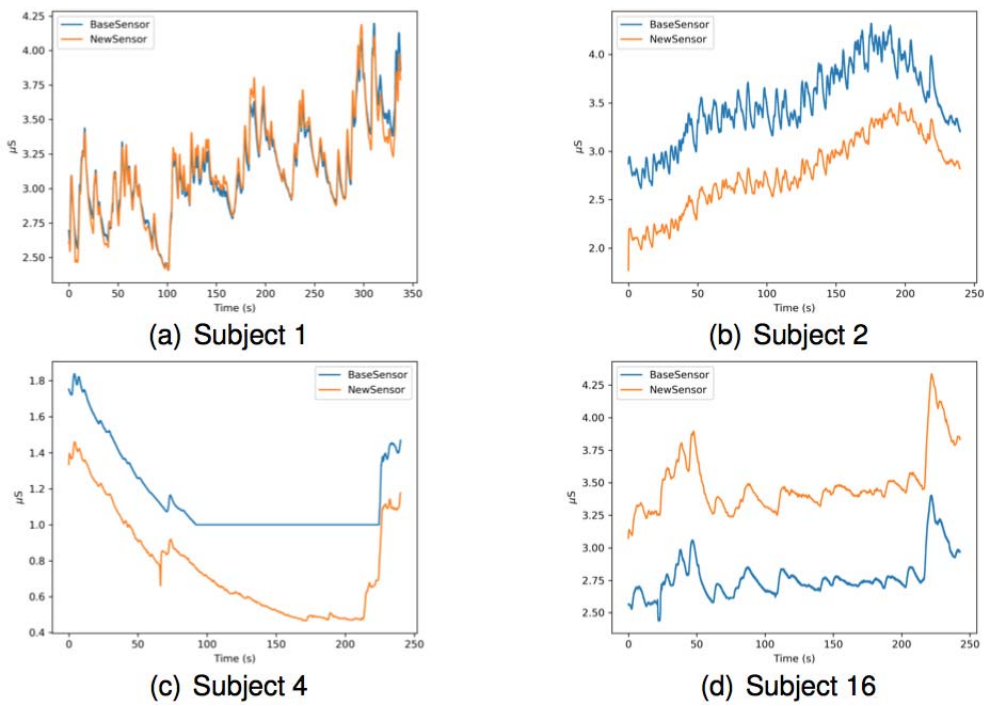


Fig. 12. Reconstructed EDA, in conductivity units (μS), comparing the reference (base) and proposed (new) sensors.

In the first case, we have the same limitations that the reference sensor has, where it can not adapt its measurement range to the target skin. As an example, on Subject 10, there are multiple variations meaning the existence of an EDR component, but the gain of this section is too high for the EDR that this subject experiences, inducing saturation at times. This is a limitation that can be solved in future work, by applying the same principle used in the first section of the new sensor design. The topology of the Sallen-Key high-pass filter enables the use of the N-MOSFET as a resistance, which, in turn, enables the control of the gain as well its frequency response. The second possible finding with these results is where we can successfully record suitable EDR data, as exemplified by the Subject 2 recording.

Figure 12 presents a portion of the EDA signals after applying the correct transfer function. As observed in Subject 4, there is a small artifact induced by the modification of the N-MOSFET equivalent resistance value. This is caused by the current dynamic gain adaptation method, which can be further improved. From Table III the overall mean for the proposed sensor was 575 compared to 624 of the reference sensor. This means that the EDA is more centered around the reference voltage in the proposed sensor, which in turns can be interpreted as using a wider dynamic range of the ADC. The median value also reinforces this evidence, with 582 on the proposed sensor against 620 on the standard sensor.

A significant comparison factor is the maximum amplitude to the mean value, where the proposed sensor scored a maximum amplitude of 135, while the reference sensor scored 94. Having more noticeable variations is generally better, since the same possible EDR will be expanded across a larger set of ADC codes, reducing the probability of not detecting EDR

events due to limitations of the ADC resolution. Finally, and using the same classification of minimum amplitude to classify an onset of a response, the proposed sensor had a comparable result to the reference sensor, but in cases where saturation occurs, obviously, from the data measured using the reference sensor it is not possible to detect EDR onsets, while with the proposed sensor it is still possible to detect EDR events to some extent.

Examining each onset in detail has shown a strong correlation in almost all detected onsets, but good to weak correlation in a minority of the onsets occur. Additionally, given the fact that EDA was being measured simultaneously in two different fingers, it was already expected that the tonic EDL measurement could differ as a consequence of local specific skin conductance at the moment of the experiment. This explains the offset between the EDA measured in Subjects 2, 4 and 16 of the plots presented in Figure 12.

V. CONCLUSION AND FUTURE WORK

The EDA contains useful information related with the sympathetic nervous system, which is at the core of several psychophysiological research areas such as affective computing or epilepsy, just to name a few. Its most significant advantage is the smaller footprint and ease of use comparatively to other biosignal modalities, however, at the instrumentation level a few limiting factors still exist.

This work contributes to address outstanding issues in EDA measurement, especially when using low-cost and open hardware platforms, by devising a sensor design with adaptive gain. The proposed circuit has shown adequate results, and in cases where saturation occurred in the adopted reference sensor, it still managed to acquire EDA signal. The dynamically

adjustable gain enables the circuit to acquire an EDA signal in all conditions, although there is still room for improvement. For example, it would be preferred if there was no need for external processing of data, and consequently have the control on the sensor itself.

The optimal condition would be one where through an onboard control logic, the sensor could adjust itself. Nonetheless, the current circuit offers the user a more flexible solution, particularly advantageous for research and to determine the best control logic, since it enables the control of the PWM output through software. Regarding the transformation to conductivity units, which is directly related with the control logic, the procedure used to calibrate the sensor can be further improved to eliminate the overall offset experienced in the sensor validation experiment, dictating a better N-MOSFET equivalent resistor value to be applied dynamically to the transfer function.

Moreover, the proposed sensor implements a new stage that separates the two EDA components. This can enable a better study of the EDA itself, and can potentially give better insights into EDRs. However, this stage suffers from multiple limitations, namely, it still has fixed gain settings, and saturates on some users. Although the high pass filter section does not have adaptive gain, contrary to the low pass configuration, it can be easily modified since it only depends on resistors. Further validation regarding the optimal cutoff frequency versus the complexity of the filter should be studied, as well as delivering adaptable gain to this stage.

Future work should continue to explore the hardware aspect in terms of electrode materials and sensor, especially improving the calibration procedure and the control logic used, focus on the development of algorithms to mitigate artifacts, and finally, explore different anatomical locations to measure electrodermal activity signals. The present work focused on further affirming the EDA as an added-value biosignal modality for everyday use scenarios.

REFERENCES

- [1] W. Boucsein, *Electrodermal Activity*. New York, NY, USA: Springer, 2012. [Online]. Available: <https://www.springer.com/gp/book/9781461411253>
- [2] A. Albraikan, D. P. Tobón, and A. E. Saddik, "Toward user-independent emotion recognition using physiological signals," *IEEE Sensors J.*, vol. 19, no. 19, pp. 8402–8412, Oct. 2019.
- [3] A. R. Butt, A. Arsalan, and M. Majid, "Multimodal personality trait recognition using wearable sensors in response to public speaking," *IEEE Sensors J.*, vol. 20, no. 12, pp. 6532–6541, Jun. 2020.
- [4] J. Malmivuo and R. Plonsey, *Bioelectromagnetism: Principles and Applications of Bioelectric and Biomagnetic Fields*. New York, NY, USA: Oxford Univ. Press, 1995.
- [5] A. Rizwan *et al.*, "Non-invasive hydration level estimation in human body using galvanic skin response," *IEEE Sensors J.*, vol. 20, no. 9, pp. 4891–4900, May 2020.
- [6] Y. S. Can *et al.*, "Real-life stress level monitoring using smart bands in the light of contextual information," *IEEE Sensors J.*, vol. 20, no. 15, pp. 8721–8730, Aug. 2020.
- [7] P. J. Bota, C. Wang, A. L. N. Fred, and H. P. da Silva, "A review, current challenges, and future possibilities on emotion recognition using machine learning and physiological signals," *IEEE Access*, vol. 7, pp. 140990–141020, 2019.
- [8] H. Critchley and Y. Nagai, *Electrodermal Activity (EDA)*. New York, NY, USA: Springer, 2013, pp. 666–669.
- [9] A. Greco, G. Valenza, L. Citi, and E. P. Scilingo, "Arousal and valence recognition of affective sounds based on electrodermal activity," *IEEE Sensors J.*, vol. 17, no. 3, pp. 716–725, Feb. 2017.
- [10] G.-J. Horng and J.-Y. Lin, "Using multimodal bio-signals for prediction of physiological cognitive state under free-living conditions," *IEEE Sensors J.*, vol. 20, no. 8, pp. 4469–4484, Apr. 2020.
- [11] H. P. da Silva, "Physiological sensing now open to the world: New resources are allowing us to learn, experiment, and create imaginative solutions for biomedical applications," *IEEE Pulse*, vol. 9, no. 2, pp. 9–11, Mar./Apr. 2018.
- [12] A. I. Faisal, S. Majumder, R. Scott, T. Mondal, D. Cowan, and M. J. Deen, "A simple, low-cost multi-sensor-based smart wearable knee monitoring system," *IEEE Sensors J.*, early access, Dec. 14, 2020, doi: [10.1109/JSEN.2020.3044784](https://doi.org/10.1109/JSEN.2020.3044784).
- [13] D. S. Lee, T. W. Chong, and B. G. Lee, "Stress events detection of driver by wearable glove system," *IEEE Sensors J.*, vol. 17, no. 1, pp. 194–204, Jan. 2017.
- [14] A. Borrego, J. Latorre, M. Alcañiz, and R. Llorens, "Reliability of the Empatica E4 wristband to measure electrodermal activity to emotional stimuli," in *Proc. Int. Conf. Virtual Rehabil.*, Jul. 2019, pp. 21–24.
- [15] C. McCarthy, N. Pradhan, C. Redpath, and A. Adler, "Validation of the Empatica E4 wristband," in *Proc. IEEE EMBS Int. Student Conf. (ISC)*, May 2016, pp. 1–4.
- [16] M.-Z. Poh, N. C. Swenson, and R. W. Picard, "A wearable sensor for unobtrusive, long-term assessment of electrodermal activity," *IEEE Trans. Biomed. Eng.*, vol. 57, no. 5, pp. 1243–1252, May 2010.
- [17] G. Pope *et al.*, "An ultra-low resource wearable EDA sensor using wavelet compression," in *Proc. IEEE 15th Int. Conf. Wearable Implant. Body Sensor Netw. (BSN)*, Mar. 2018, pp. 193–196.
- [18] R. Picard and J. Scheirer, "The galvactivator: A glove that senses and communicates skin conductivity," MIT Media Lab, Cambridge, MA, USA, Tech. Rep. TR-542, 2001. [Online]. Available: <https://www.media.mit.edu/publications/the-galvactivator-a-glove-that-senses-and-communicates-skin-conductivity-2/>
- [19] Y. B. Lee, S. W. Yoon, C. K. Lee, and M. H. Lee, "Wearable EDA sensor gloves using conducting fabric and embedded system," in *Proc. Int. Conf. IEEE Eng. Med. Biol. Soc. (EMBC)*, Aug./Sep. 2006, pp. 6785–6788.
- [20] R. R. Fletcher *et al.*, "ICalm: Wearable sensor and network architecture for wirelessly communicating and logging autonomic activity," *IEEE Trans. Inf. Technol. Biomed.*, vol. 14, no. 2, pp. 215–223, Mar. 2010.
- [21] J. Sousa, H. P. da Silva, N. Santos, and P. Aires, "Smart wearable sensors for biomedical data monitoring in the treatment of depression," in *Proc. Int. eHealth, Telemed. Health Forum (ICT, Med-e-Tel)*, 2012, p. 122.
- [22] J. Jussila, N. Venho, H. Saloniemi, J. Moilanen, J. Liukkonen, and M. Rinnetmäki, "Towards ecosystem for research and development of electrodermal activity applications," in *Proc. Int. Academic Mindtrek Conf.*, Oct. 2018, pp. 79–87.
- [23] H. P. da Silva, A. Fred, and R. Martins, "Biosignals for everyone," *IEEE Pervasive Comput.*, vol. 13, no. 4, pp. 64–71, Oct. 2014.
- [24] D. Batista, H. P. da Silva, A. Fred, C. Moreira, M. Reis, and H. A. Ferreira, "Benchmarking of the BITalino biomedical toolkit against an established gold standard," *Healthcare Technol. Lett.*, vol. 6, no. 2, pp. 32–36, Apr. 2019.
- [25] K. Kutt, W. Binek, P. Misiak, G. Nalepa, and S. Bobek, *Towards the Development of Sensor Platform for Processing Physiological Data From Wearable Sensors*. Cham, Switzerland: Springer, 2018, pp. 168–178.
- [26] W. Boucsein *et al.*, "Publication recommendations for electrodermal measurements," *Psychophysiology*, vol. 49, no. 8, pp. 1017–1034, 2012.
- [27] A. Sedra and K. Smith, *Microelectronic Circuits*. London, U.K.: Oxford Univ. Press, 2009.
- [28] J. Guerreiro, "A biosignal embedded system for physiological computing," M.S. thesis, Dept. Electron., Telecommun. Comput. Eng., ADEETC, Instituto Superior de Engenharia de Lisboa, Lisbon, Portugal, 2013.
- [29] M. Schmidt, D. Penner, A. Burkl, R. Stojanovic, T. Schümann, and P. Beckerle, "Implementation and evaluation of a low-cost and compact electrodermal activity measurement system," *Measurement*, vol. 92, pp. 96–102, Oct. 2016.
- [30] A. Zygmunt and J. Stanczyk, "Methods of evaluation of autonomic nervous system function," *Arch. Med. Sci.*, vol. 6, no. 1, pp. 11–18, Mar. 2010.



António Rodrigues Banganho received the B.S. degree in biomedical engineering from the Instituto Superior de Engenharia de Coimbra (ISEC), Instituto Politécnico de Coimbra (IPC), Portugal, and the M.Sc. degree in electrical and computer engineering from the Instituto Superior Técnico (IST), Universidade de Lisboa (UL), Portugal.



Hugo Plácido da Silva (Senior Member, IEEE) received the Ph.D. degree in electrical and computer engineering from IST-UL. Since 2004, he has been a Researcher with the Instituto de Telecomunicações (IT). He is currently a Professor with IST-UL. His current interests include biomedical research, systems engineering, signal processing, and pattern recognition. His work has been internationally distinguished with several academic and technical awards.



Marcelino Bicho dos Santos (Senior Member, IEEE) is currently the CTO and Co-Founder of SiliconGate, a power management IP design company. He is also a Professor with IST-UL and also a Researcher with INESC-ID. His current interests include low power design and general power management solutions including voltage regulators, reference voltage and reference current generation, ultralow power PMUs, dynamic voltage, frequency scaling, and power gating.